Cancer Screening and Prevention **2025** vol. 4(2) | 79–88
DOI: 10.14218/CSP.2025.00004

Original Article

Diagnostic Performance of ATR-FTIR Spectroscopy in Discriminating Normal Breast Tissue and Breast Tumors

Samuel T. Adeleke[1*], Christopher Igbeneghu[2] and Sina Iyiola[3]

[1]Department of Medical Laboratory Science, Bowen University, Iwo, Osun State, Nigeria; [2]Department of Medical Laboratory Science, Ladoke Akintola University of Technology, Ogbomoso, Oyo State, Nigeria; [3]Department of Medical Laboratory Science, Achievers University, Owo, Ondo State, Nigeria

Received: January 30, 2025 | **Revised:** March 27, 2025 | **Accepted:** April 27, 2025 | **Published online:** May 26, 2025

Abstract

Background and objectives: Histopathology is the gold standard in cancer diagnosis. However, attenuated total reflectance (ATR)-Fourier transform infrared (FTIR) spectroscopy has shown diagnostic potential in other settings. Therefore, this study aimed to investigate the sensitivity and specificity of the ATR-FTIR spectroscopy in evaluating breast lesions.

Methods: This study was conducted on formalin-fixed, paraffin-embedded biopsy blocks received at Ladoke Akintola University of Technology Teaching Hospital between 2022 and 2023. The blocks were categorized into 10 normal (from benign breast tissue), 15 benign, and 31 malignant samples. Tissue sections of 15 µm were obtained during block trimming and floated onto FTIR slides. An additional 4 µm tissue sections were stained with hematoxylin and eosin for tumor diagnosis and to identify suitable areas on the FTIR slide. Spectrometer readings were taken within the range of 4,000–600 cm^{-1}, 32 scans, and 16 cm^{-1} resolution, using the average of 10 preprocessed spectra per slide. Biomarkers were calculated by ratioing peak intensities for A1632/A1543, A1632/A2922, A1632/A1080, A1080/A1543, A1237/A1080, and A1043/A1543, which represent protein, diagnostic marker, cytoplasm-nucleus ratio, carcinogenesis marker, phosphate, and glycogen, respectively. The receiver operating characteristic curve was used to determine sensitivity, specificity, and the area under the curve (AUC).

Results: The AUC analysis showed that cytoplasm-nucleus ratio values of 0.99 and 0.95 effectively distinguished normal from malignant tissue, and benign from malignant tissue, respectively ($p < 0.0001$). Additionally, protein marker (AUC = 0.73), diagnostic marker (AUC = 0.85), and cytoplasm-nucleus ratio marker (AUC = 0.94) were able to discriminate normal from benign tissue. Overall, the receiver operating characteristic analysis showed 100% sensitivity and specificity ranging from 54% to 87%. Glycogen (AUC = 1.00) exhibited 100% sensitivity in discriminating fibroadenoma from fibrocystic changes.

Conclusions: ATR-FTIR spectroscopy demonstrates high diagnostic accuracy in differentiating normal, benign, and malignant breast tissues using specific spectral biomarkers. Among these, the cytoplasm-nucleus ratio marker showed strong potential as a reliable spectral indicator for distinguishing various types of breast tumors. The cytoplasm-nucleus ratio marker demonstrated strong potential as a reliable spectral indicator for distinguishing various types of breast tumors.

Introduction

The breast holds significant importance in the reproductive aspects of women, while serving a more limited role in men. Its structure primarily consists of epithelium and stroma, with the terminal duct-lobular unit (TDLU) functioning as the essential component of the epithelial structure. The TDLU facilitates both secretory and collection functions during lactation.[1] This unit is critical in reactive adaptations to physiological demands; however, most pathological lesions originate from epithelial cells in the TDLU area.[2] Lesions are typically classified into benign and malignant categories, with benign conditions predominantly exhibiting inflammatory characteristics, epithelial hyperplasia, adenomas, fibrocystic changes, and fibroadenomas. Conventional diagnostic approaches, primarily reliant on histopathology of breast tissue, are limited by inconsistencies stemming from subjective interpretation and variability among pathologists.[3,4] Consequently, there is a demonstrat-

Keywords: Terminal duct-lobular unit; TDLU; Fibroadenoma; Fibrocystic; Sensitivity; Specificity; Biomarkers; Area under the curve; Peak ratio; Point mapping; Performance; Invasive ductal cancer.

[*]**Correspondence to:** Samuel T. Adeleke, Department of Medical Laboratory Sciences, Bowen University, Iwo, Osun State 232102, Nigeria. ORCID: https://orcid.org/0000-0001-9912-9573. Tel: +234-8133114950, E-mail: samuel.adeleke@bowen.edu.ng

How to cite this article: Adeleke ST, Igbeneghu C, Iyiola S. Diagnostic Performance of ATR-FTIR Spectroscopy in Discriminating Normal Breast Tissue and Breast Tumors. *Cancer Screen Prev* 2025;4(2):79–88. doi: 10.14218/CSP.2025.00004.

ed need for the integration of objective methodologies to enhance diagnostic accuracy and reliability.

Fourier-transform infrared (FTIR) spectroscopy is a technique that involves exposing a sample to infrared light while measuring the energy that either passes through or reflects from the sample as a function of wavenumbers.[5,6] During this process, infrared-active functional groups within biomolecules absorb the energy from the incoming light.[3] Studies by Elshemey *et al*.[4] and Luo *et al*.[5] highlight FTIR spectroscopy's sensitivity to various biomolecules, enabling it to generate biochemical signatures that differentiate proteins, lipids, and nucleic acids based on the distinct vibration energy requirements of their functional groups.[4–6] Characteristic features like peak shapes, heights, and ratios are utilized for both qualitative and quantitative assessments of the samples.[5–7]

Consequently, FTIR spectroscopy emerges as a powerful diagnostic tool, with clinical applications extending beyond screening and diagnosis to the ongoing monitoring of treatment responses. Its use has been documented in analyzing diverse clinical samples, including formalin-fixed paraffin-embedded tissues, as well as cases associated with disorders like diabetes and gastric cancer,[8,9] neurodegenerative diseases such as Alzheimer's,[10] and conditions like atherosclerosis,[11] and breast cancer.[12]

Among FTIR techniques, attenuated total reflectance (ATR) spectroscopy is particularly prevalent. It typically employs a diamond to gather data from the layer of the sample adjacent to the internal reflection element surface.[11,12] Its higher signal-to-noise ratio and reduced scattering make ATR more efficient for biological material assessments, combined with minimal sample preparation since infrared light penetration depth remains unaffected by sample thickness.

While FTIR spectroscopy is increasingly utilized in Nigeria and Sub-Saharan Africa, its application to biological tissues, particularly in cancer research, remains limited.[13–16] Prior studies on breast cancer using vibrational spectroscopy have primarily been conducted outside the region,[17,18] and local investigations are scarce. To date, only X-ray emission techniques have been employed in Nigeria to differentiate between cancerous and non-cancerous breast tissues.[19] Therefore, this pioneering study aimed to evaluate the diagnostic accuracy of ATR-FTIR spectroscopy in differentiating normal, benign, and malignant breast lesions in a Nigerian population, identifying specific spectral signatures for tumor discrimination.

Materials and methods

Ethical consideration

Ethical approval for the study was granted by the Research Ethics Committee of Ladoke Akintola University of Technology (LAUTECH), Osun, Nigeria, with reference number: UTH/REC/2022/09/649. The study was carried out with a waiver of informed consent for the use of archived, anonymized samples in accordance with the principles of the Declaration of Helsinki (as revised in 2024). The ethics committee agreed that this study did not require informed consent due to its retrospective nature and the minimal risk involved.

Tissue retrieval and sorting

This retrospective study, conducted at LAUTECH, analyzed formalin-fixed paraffin-embedded biopsy samples from female patients collected between 2022 and 2023. The sample set included 10 normal breast samples, 15 benign samples (fibroadenoma and fibrocystic changes), and 31 malignant specimens (invasive ductal carcinoma grade II) as shown in Figures 1 and 2. Using quota sampling, only primary tumors with complete information and that had not undergone neoadjuvant therapy during the study period were included.

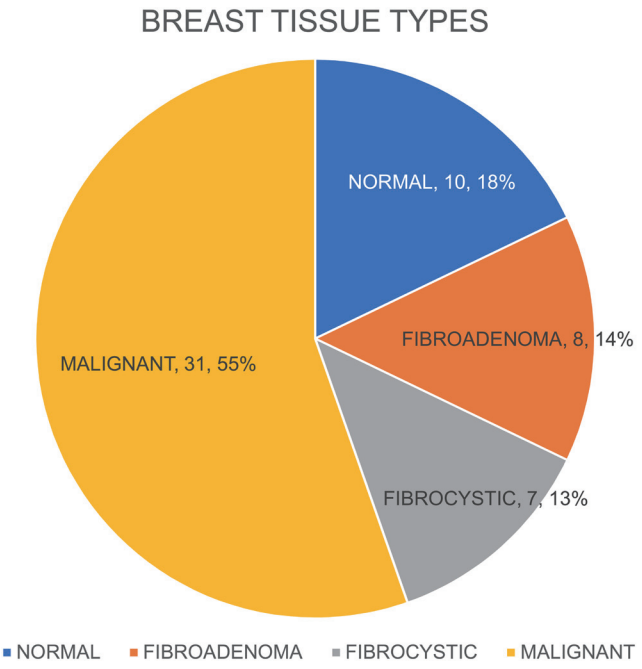

Fig. 1. Percentage proportion of normal (18%), fibroadenoma (14%), fibrocystic (13%), and malignant (invasive ductal cancer grade II) (55%) breast tissue.

Tissue section preparation

Tissue sections measuring 15 µm were prepared from sorted tissue blocks using a Leica RM2125 microtome and transferred to aluminum foil substrates adapted for spectral acquisition according to Cui *et al*.[20] An additional 4 µm section was stained with hematoxylin and eosin using a standard procedure.[21] Tumor classification and identification of suitable areas were performed by two pathologists in a blinded study prior to FTIR analysis.

ATR-FTIR spectroscopic analysis on tissue samples

Following heat treatment at 55–60°C to dry the tissue sections, xylene (Surgipath Medical Industries, Inc.) was used for deparaffinization, followed by a descending ethanol series (Sigma-Aldrich) for rehydration, and then atmospheric drying. The Cary 630 Agilent spectrometer was calibrated against blank substrates before spectral acquisition. Point mapping was conducted on tissue sections placed on low-reflective slides as substrates, ensuring precise contact with the diamond ATR crystal at pre-defined normal and tumorous regions, previously annotated, following a methodology adapted from Baker *et al*.[22] The tissue section fields were scanned across the mid-infrared range of 4,000 cm^{-1} to 600 cm^{-1}, accumulating 32 scans at a resolution of 16 cm^{-1} and averaging ten spectra for each specimen. Spectra were preprocessed through baseline corrections and smoothing techniques. Peaks and their relative intensities were identified, and spectral biomarkers corresponding to specific peak ratios were analyzed: A2922/A1632, A1632/A1543, A1632/A1080, A1080/A1543, and A1237/A1080, which were identified

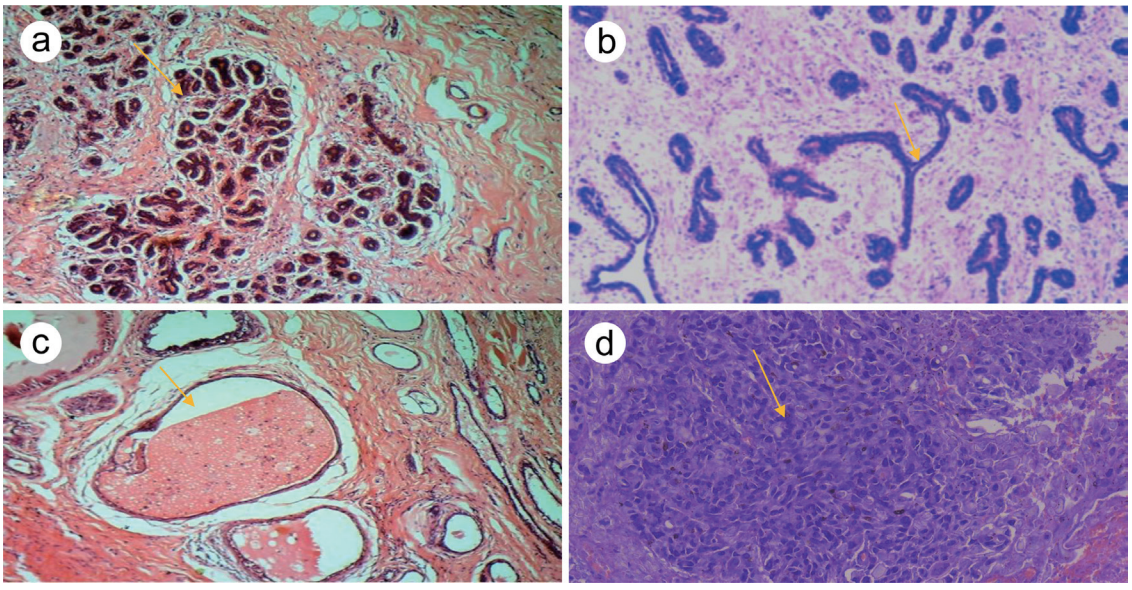

Fig. 2. Haematoxylin and Eosin stained photomicrographs of (a) normal breast tissue section with lobules containing dark blue-stained acini nuclei (black arrow), separated by denser collagen fibers, compared with the stroma that separates the lobules ×400. (b) Breast lobules compressed into a slit-like shape (star-black arrow) due to excessive growth of the intervening stroma that separates the lobules (Fibroadenoma) ×400. (c) Cystic breast tissue with two large cysts (black arrow) filled with pink-staining amorphous material, lined by a single layer of epithelial cells ×400. (d) Invasive ductal carcinoma (Not Special Types). This case was Nottingham grade II. Note the number of tubule formations, high pleomorphism, and mitotic figures in the picture ×400.

as biomarkers for diagnostic marker (DM),[4] protein,[5] cytoplasmic-nuclear ratio (CN),[23] carcinogenesis markers,[24] phosphate,[25] and glycogen,[26] respectively as depicted in Figures 3 and 4.

Statistical analysis

Average values of these biomarkers were compared across normal, fibroadenoma, fibrocystic changes, and invasive ductal carcinoma grade 2 tissues, as displayed in Figure 3. Receiver operating characteristic (ROC) curves were employed to assess the sensitivity, specificity, and performance of the spectral biomarkers.[4–6] The performance was quantified using area under the curve (AUC) metrics, where values < 0.5 indicate no discrimination, 0.5 represents random guessing, 0.6–0.7 indicates low discrimination, 0.7–0.8 signifies moderate discrimination, and scores between 0.9–1.0 denote excellent discriminatory capability. Data visualization and analysis were conducted using Microsoft Excel and SPSS 26, with results presented in both tables and graphs. Significance was set at a 95% confidence level ($p < 0.05$).

Results

Distribution of breast tissue types

In the study, the sampled breast tissue types were categorized into

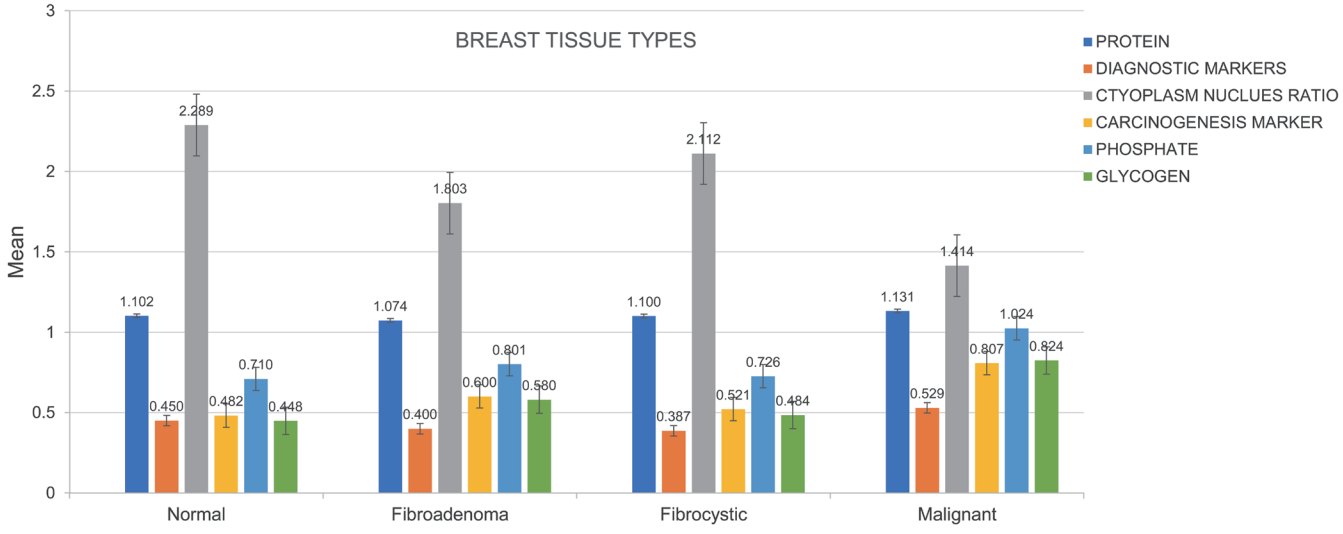

Fig. 3. Mean distribution of spectral biomarkers among normal, fibroadenoma, fibrocystic, and malignant breast tissues (invasive ductal cancer grade II).

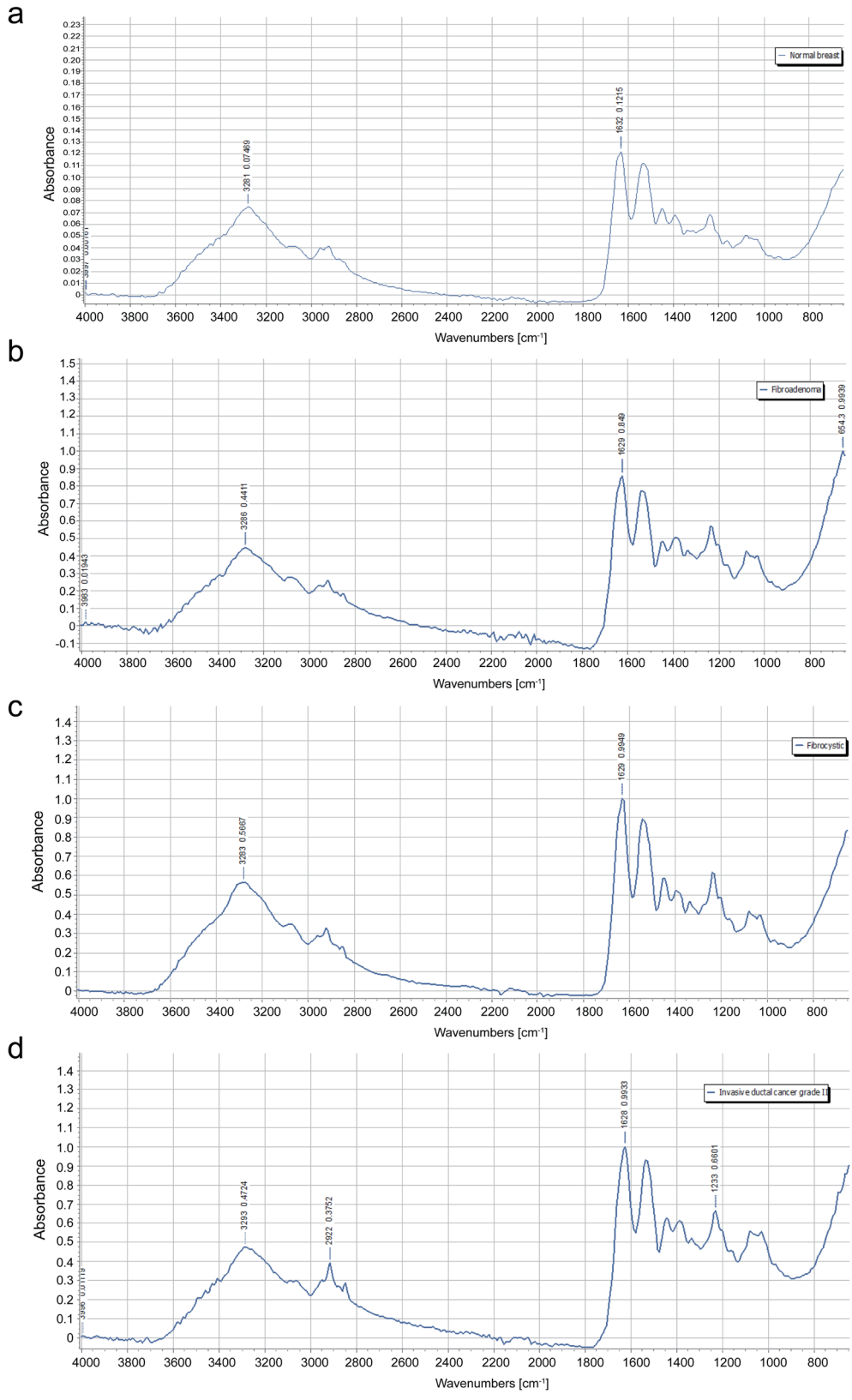

Fig. 4. Spectra of (a) normal breast tissue showing peak positions and peak intensities, (b) breast fibroadenoma showing peak positions and peak intensities, (c) fibrocystic breast disease showing peak positions and peak intensities, (d) invasive breast cancer grade 2 showing peak positions and peak

Table 1. Model performance of biomarkers between normal breast tissue and fibroadenoma

	Area	SE	95% CI		*p*-value
			Lower bound	Upper bound	
Protein	0.810**	0.142	0.53	1.000	0.138
DM	0.810**	0.179	0.466	1.000	0.138
CN	1.000***	0.001	1.000	1.000	0.017
CM	0.048	0.069	0.001	0.183	0.03
Phosphate	0.095	0.107	0.001	0.305	0.053
Glycogen	0.001	0.000	0.001	0.001	0.017

In discriminating between normal breast tissue and fibroadenoma using AUC values, we found that the cytoplasm:nucleus ratio showed excellent diagnostic performance (1.00) at $p = 0.017$. Protein and diagnostic markers showed moderate diagnostic performance (0.810) at $p = 0.138$ as shown in Figure S1. Carcinogenesis (AUC = 0.048, $p = 0.03$), phosphate (AUC = 0.095, $p = 0.05$), and glycogen (AUC = 0.001, $p = 0.017$) however lacked diagnostic ability. **moderate diagnostic performance; ***excellent diagnostic performance. AUC, area under the curve; CI, confidence interval; CM, carcinogenesis marker; CN, cytoplasmic:nucleus ratio; DM, diagnostic marker; SE, standard error.

ten normal, eight fibroadenoma, seven fibrocystic, and 31 malignant samples, as shown in Figure 1 below. The photomicrographs also showed the characteristics of different breast tissue types (Fig. 2).

Mean distribution of spectral biomarkers

The mean distribution of biomarkers was assessed across normal breast, fibroadenoma, fibrocystic, and malignant breast tissues, with the results presented in Figure 3. This provides a graphical highlight of how biomarkers differ among different breast tissue categories (normal and abnormal).

Quantitative determination of spectral biomarkers attributed to cytoplasm: nucleus ratios was particularly elevated in normal breast tissue (2.29), followed by fibrocystic (2.11), fibroadenoma (1.80), and lowest in malignant tissue (1.41). Similarly, glycogen levels were highest in malignant breast tissue (0.82), followed by fibroadenoma (0.58), fibrocystic (0.484), and normal (0.448). The carcinogenesis marker showed an increase in cancer tissue (0.81), relative to fibroadenoma (0.60), fibrocystic (0.52), and normal (0.48). Phosphate followed a similar pattern, with higher levels in malignant breast tissue compared to fibroadenoma, fibrocystic, and normal tissues. Protein and diagnostic markers in malignant, fibroadenoma, fibrocystic, and normal breast tissues were 1.31, 1.07, 1.10, and 1.10, and 0.53, 0.40, 0.39, and 0.45, respectively. The general trend of results showed that invasive ductal carcinoma and fibroadenoma exhibited elevated biomarkers compared to fibrocystic and normal breast tissue, suggesting differences in the degree of differentiation between these groups.

Diagnostic model performance on matched breast samples

To ascertain the diagnostic plausibility of biomarkers in discriminating between normal and fibroadenoma, normal and fibrocystic, normal and malignant breast tissue, fibroadenoma and malignant, fibrocystic and malignant, and fibroadenoma and fibrocystic tissues, ROC was performed to highlight the discriminatory power of these biomarkers within a 95% confidence interval, as presented in Tables 1–6. Furthermore, the sensitivity and specificity of these biomarkers were evaluated to assess their ability to detect true positives (cancer cases) and rule out false positives (non-cancer cases) (Table 7).

Table 7 shows the sensitivity and specificity of matched binary samples. Generally, the CN marker demonstrated exceptional performance, achieving 100% sensitivity in differentiating normal breast tissue from both benign (fibroadenoma and fibrocystic) and malignant lesions as shown in Figure S6. The protein marker also yielded 100% sensitivity when distinguishing normal tissue from fibroadenoma, although it exhibited a specificity of 71%. Additional markers, including the DM, carcinogenesis marker, phosphate, and glycogen, exhibited 100% specificity across most tumors but displayed variability in sensitivity, ranging from 45% to 75%. The CN marker also achieved perfect discrimination between normal breast tissue and fibroadenoma, maintaining both sensitivity and

Table 2. Model performance of biomarkers between normal breast and fibrocystic breast tissues

	Area	SE	95% CI		*p*-value
			Lower bound	Upper bound	
Protein	0.583	0.237	0.119	1.000	0.724
DM	0.917***	0.115	0.691	1.000	0.077
CN	0.833**	0.173	0.493	1.000	0.157
CM	0.083	0.115	0.001	0.309	0.077
Phosphate	0.333	0.272	0.001	0.867	0.480
Glycogen	0.001	0.000	0.001	0.001	0.034

In discriminating between normal breast and fibrocystic breast tissues using AUC values, we found that the cytoplasm:nucleus ratio showed moderate diagnostic performance (AUC = 0.833) at $p = 0.157$. The diagnostic marker showed excellent diagnostic performance (AUC = 0.917) at $p = 0.077$. Other biomarkers such as protein (AUC = 0.583, $p = 0.724$), carcinogenesis (AUC = 0.083, $p = 0.077$) as shown in Figure S2, phosphate (AUC = 0.33, $p = 0.48$), and glycogen (AUC = 0.001, $p = 0.034$) had weak performance and were most likely unreliable for diagnosis. **moderate diagnostic performance; ***excellent diagnostic performance. AUC, area under the curve; CI, confidence interval; CM, carcinogenesis marker; CN, cytoplasmic:nucleus ratio; DM, diagnostic marker; SE, standard error.

Table 3. Model performance of biomarkers between normal breast and malignant (invasive ductal carcinoma grade 2) breast tissues

	Area	SE	95% CI		*p*-value
			Lower bound	Upper bound	
Protein	0.305	0.075	0.158	0.458	0.256
DM	0.208	0.087	0.038	0.377	0.089
CN	0.990***	0.012	0.965	1.000	0.004
CM	0.001	0.001	0.01	0.01	0.004
Phosphate	0.005	0.008	0.001	0.02	0.004
Glycogen	0.005	0.008	0.001	0.02	0.004

In discriminating between normal breast and malignant (invasive ductal carcinoma) breast tissues using AUC values, we found that the cytoplasm:nucleus ratio revealed perfect diagnostic performance (AUC = 0.99, $p = 0.004$) as shown in Figure S3, whereas other biomarkers such as protein, diagnostic marker, carcinogenesis marker, phosphate, and glycogen had AUC values below 0.5 and *p*-values less than 0.05. ***excellent diagnostic performance. AUC, area under the curve; CI, confidence interval; CM, carcinogenesis marker; CN, cytoplasmic:nucleus ratio; DM, diagnostic marker; SE, standard error.

Table 4. Model performance of biomarkers between fibroadenoma and malignant (invasive ductal carcinoma grade 2) breast tissues

	Area	SE	95% CI		*p*-value
			Lower bound	Upper bound	
Protein	0.148	0.057	0.036	0.259	0.002
DM	0.025	0.017	0.01	0.059	0.001
CN	0.935***	0.028	0.088	0.991	0.001
CM	0.037	0.021	0.001	0.077	0.001
Phosphate	0.0081	0.013	0.001	0.043	0.001
Glycogen	0.041	0.022	0.001	0.084	0.001

In discriminating between fibroadenoma and malignant breast tissues using AUC values, we found that the cytoplasm:nucleus ratio showed excellent diagnostic performance (AUC = 0.935, $p = 0.001$, statistical significance) as shown in Figure S4. The remaining biomarkers were less than optimal, with AUC < 0.5 and $p < 0.005$. ***excellent diagnostic performance. AUC, area under the curve; CI, confidence interval; CM, carcinogenesis marker; CN, cytoplasmic:nucleus ratio; DM, diagnostic marker; SE, standard error.

specificity at 100%. While the protein and DM markers similarly differentiated normal tissue from fibroadenoma with 100% sensitivity, other markers did not reach notable performance levels (Table 1). Overall, the CN marker effectively distinguished normal from malignant, benign lesions like fibroadenoma and fibrocystic changes from malignant lesions; all with sensitivities of 100% and differing specificities of 69%, 86% and 97% respectively (Tables 2–5). Glycogen was particularly a useful discriminator between fibrocystic and fibroadenoma with 100% sensitivity and specificity (Table 6). Other markers provided limited to moderate discriminatory information as revealed in Tables 1–7.

ROC curve analysis, by identifying optimal threshold values, demonstrated its capacity to distinguish between distinct breast cancer classifications. Cytoplasmic-nuclear ratios, with cut-offs ranging from 2.08 to 2.10, effectively differentiated between normal tissue and fibroadenomas/fibrocystic, invasive ductal carcinoma, and normal/fibroadenoma. A diagnostic marker cut-off of 0.39 proved useful in discriminating between normal and fibroadenomatous/fibrocystic tissues, as well as between fibroadenomas and fibrocystic tissues (Table 7).

Table 5. Model performance of biomarkers between fibrocystic and malignant (invasive ductal carcinoma grade 2) breast tissues

	Area	SE	95% CI		*p*-value
			Lower bound	Upper bound	
Protein	0.298	0.088	0.125	0.47	0.177
DM	0.008	0.01	0.001	0.028	0.001
CN	0.976***	0.019	0.94	1.000	0.001
CM	0.008	0.01	0.001	0.027	0.001
Phosphate	0.001	0.001	0.001	0.002	0.001
Glycogen	0.004	0.006	0.001	0.016	0.001

In discriminating between fibrocystic and malignant breast tissues using AUC values, we found that the cytoplasm:nucleus ratio showed excellent diagnostic performance (AUC = 0.976, $p = 0.001$, statistical significance) as shown in Figure S4. The remaining biomarkers were less than optimal, with AUC values < 0.5 and $p < 0.005$. ***excellent diagnostic performance. AUC, area under the curve; CI, confidence interval; CM, carcinogenesis marker; CN, cytoplasmic:nucleus ratio; DM, diagnostic marker; SE, standard error.

Table 6. Model performance of biomarkers between fibrocystic and fibroadenoma breast tissues

	Area	SE	95% CI		*p*-value
			Lower bound	Upper bound	
Protein	0.214	0.15	0.001	0.508	0.131
DM	0.643*	0.174	0.301	0.984	0.45
CN	0.071	0.082	0.001	0.232	0.023
CM	0.857**	0.132	0.598	1.000	0.059
Phosphate	0.821**	0.137	0.552	1.000	0.089
Glycogen	1.000***	0.001	1.000	1.000	0.008

In discriminating between fibrocystic breast and fibroadenoma breast tissues using AUC values, we found that the cytoplasm:nucleus ratio, though statistically significant, did not show much diagnostic power, with an AUC of 0.07, implying no significant changes in the cytoplasm:nucleus morphometry between fibroadenoma and fibrocystic breast tissues. However, a fair diagnostic performance was observed with the diagnostic marker (AUC = 0.643, $p = 0.45$); moderate diagnostic performance was found with both carcinogenesis marker (AUC = 0.857, $p = 0.059$) and phosphate (AUC = 0.821, $p = 0.089$). Glycogen, on the other hand, showed perfect diagnostic performance, with an AUC of 1.00 at $p = 0.008$ (statistical significance) as shown in Figure S5. *fair diagnostic performance; **moderate diagnostic performance; ***excellent diagnostic performance. AUC, area under the curve; CI, confidence interval; CM, carcinogenesis marker; CN, cytoplasmic:nucleus ratio; DM, diagnostic marker; SE, standard error.

Table 7. Peak ratios, important biomarker assignment, sensitivity, specificity, and cut-off points of comparison among normal, fibroadenoma, fibrocystic, and malignant breast tissues

Histology classification	Peak ratios	Biomarker assignment	Sensitivity%	Specificity%	Cut-off points
Normal					
Malignant	A1632/A1080	CN	100	69	2.10
Fibroadenoma					
Malignant	A1632/A1080	CN	100	86	1.58
Fibrocystic					
Malignant	A1632/A1080	CN	100	97	2.10
Normal					
Fibroadenoma	A1632/A1535	Protein	100	71	1.09
Normal					
Fibroadenoma	A2922/A1632	DM	100	43	0.39
Normal					
Fibroadenoma	A1632/A1080	CN	100	100	2.10
Normal					
Fibrocystic	A2922/A1632	DM	100	75	0.39
Normal					
Fibrocystic	A1632/A1080	CN	100	50	2.08
Fibroadenoma					
Fibrocystic	A2922/A1632	DM	71	75	0.39
Fibroadenoma					
Fibrocystic	A1080/A1543	CM	86	100	0.54
Fibroadenoma					
Fibrocystic	A1237/A1080	Phosphate	82	100	0.77
Fibroadenoma					
Fibrocystic	A1043/A1543	Glycogen	100	100	0.51

CM, carcinogenesis marker; CN, cytoplasmic:nucleus ratio; DM, diagnostic marker.

Discussion

The current study analyzed breast tissue classified histopathologically as normal, benign (fibroadenoma and fibrocystic), and malignant using ATR-FTIR spectroscopy to identify spectral peak intensities as potential biomarkers for proteins, diagnostic markers, carcinogenesis markers, cytoplasmic-nuclear ratios, phosphate, and glycogen. A ROC curve statistical analysis validated these biomarkers based on their ability to distinguish various breast tissue types. In particular, biomarkers demonstrating high discriminatory power, as reflected in AUC values, were prioritized. The AUC offers a definitive assessment of a model's performance, often surpassing mere measurements of diagnostic accuracy.[27–30] Thus, ROC curve analysis was systematically employed across the selected biomarkers to establish their respective sensitivities, specificities, AUCs, and cut-off points when contrasting breast tissue types.

ROC curve analysis provides a visual and quantitative method for evaluating overall test performance by plotting sensitivity against specificity. The AUC reflects the test's overall diagnostic effectiveness, balancing the two metrics. Values below 0.5 suggest no discrimination capability, while values between 0.5 and 0.6 indicate random chance. AUCs from 0.6 to 0.7 reflect marginal discrimination ability, 0.7 to 0.8 suggest moderate discrimination, and those above 0.9 indicate excellent discrimination.[29,30]

Sensitivity measures the likelihood of accurately identifying diseased patients, while specificity assesses the capability of a test to exclude healthy individuals correctly.[4,6] The necessity to reduce the proportion of false positives is crucial in ensuring proper screening for positive subjects.[27,28] Our findings indicate that ATR-FTIR successfully differentiated nearly all breast tumor classes per histopathological classification. In Table 3 and Table 7, the CN ratio, shown by the peak ratio A1632/A1080, was significantly elevated in normal compared to malignant tissues ($p = 0.04$, AUC = 0.990, sensitivity = 100%, specificity = 69%). This ratio also demonstrated remarkable discriminatory ability ($p = 0.017$; AUC = 1.00, sensitivity = 100%, specificity = 100%) between normal and fibroadenoma, as shown in Table 1 and Table 7. Moreover, the protein peak ratio A1632/A1543 in Tables 1 and 7 showed an AUC of 0.810 with sensitivities of 100% and specificities of 71% ($p = 0.138$). Conversely, the diagnostic marker (A2922/A1632) showed promise, achieving AUC = 0.810, specificity = 43% ($p = 0.138$) with 100% sensitivity in Tables 1 and 7.

Additionally, in Tables 2 and 7, the diagnostic marker (AUC = 0.917, sensitivity = 100%, specificity = 75% at $p = 0.077$) and the cytoplasmic-nuclear ratio (AUC = 0.833, sensitivity = 100%, specificity = 50% at $p = 0.157$) indicated considerable efficacy in differentiating normal from fibrocystic tissue, showcasing the latter's specific superiority in this regard. The cytoplasmic-nuclear ratio exhibited excellent performance (AUC = 0.935, sensitivity = 100%, specificity = 86%, $p = 0.01$) in differentiating between fibroadenoma and malignant tumors, as shown in Tables 4 and 7, as well as between fibrocystic and malignant tissues (AUC = 0.976, sensitivity = 100%, specificity = 97%, $p = 0.01$) seen in Tables 5 and 7. In discerning fibrocystic changes from fibroadenoma, as shown in Tables 6 and 7, the glycogen peak displayed outstanding discriminatory capability (AUC = 1.0, sensitivity = 100%, specificity = 100%), outperforming the carcinogenic marker (AUC = 0.857, $p = 0.059$, sensitivity = 86%, specificity = 100%) and phosphate marker (AUC = 0.821, $p = 0.089$, sensitivity = 82%, specificity = 100%). The weakest performance, with sensitivity at 71% and specificity at 75% along with an AUC of 0.643 and no significance ($p = 0.45$), was observed in the diagnostic marker.

The study identified the cytoplasmic-nuclear ratio's diagnostic potential, particularly in distinguishing malignant breast tissues from normal and benign types, illustrating its importance in the clinical diagnostic landscape. The cytoplasmic-nuclear ratio has traditionally been vital in histopathological diagnoses,[1,2] validated by various analytical methods.[31–33] This marker exhibited high specificity (100%) for differentiating normal from both fibroadenoma and malignant tissues, suggesting a closer similarity between normal breast tissues and fibrocystic changes, as supported by existing literature.[34]

While the peak ratio A2922/A1650 has exhibited diagnostic capability in previous studies, approaching AUC values of 0.908 and 100% sensitivity in distinguishing diseased from healthy tissues,[4,6] these findings were not uniformly observed in the present study. Similar 100% sensitivity patterns with 70% specificity and an AUC value of 0.810 were noted primarily between normal and fibroadenoma tissues. This suggests that further exploration of these biomarkers could yield significant insights into breast cancer dynamics—a notion echoed in complementary studies.[6] The protein peaks, generally assumed to elevate in cancerous tissues compared to normal counterparts, did not exhibit notable statistical significance in this study. While statistical significance was generally elusive, a particular biomarker, protein, exhibited 100% sensitivity and 69% specificity, but a low AUC of 0.325. This suggests its limited ability to differentiate between normal tissue and invasive ductal carcinoma, potentially due to the instability of the utilized β-sheet derived secondary proteins,[35,36] unlike the more stable α-sheet derived proteins used in prior studies.[37–41] This contrasts with reports demonstrating the utility of α:β ratios and Amide II/Amide III ratios in serum for distinguishing breast cancer patients from healthy subjects.[40] Variations in peak ratios from differing protein structures can impact diagnostic sensitivity, and despite high sensitivity and diagnostic performance between normal and fibroadenoma tissues, statistical significance was lacking.[33] Thus, the implementation of this protein biomarker warrants careful consideration due to its statistical insignificance, potentially stemming from confounding variables like formalin fixation.[39] Nonetheless, the observed trends suggest potential diagnostic utility.

Furthermore, the glycogen peak demonstrated elevated levels in cancerous tissues as previously reported.[35–38] Its presence during the G1 phase may enhance energy provision for tumors,[38,39] confirmed by perfect AUC = 1.00, and 100% sensitivity and specificity in this present study. Elsewhere, salivary carbohydrate profiles, specifically the peak at 1,041 cm^{-1}, have been reported to exhibit moderate diagnostic utility in breast cancer detection.[6] Ferreira *et al*.[6] reported an AUC of 0.765–0.770, with 80% sensitivity and 70% specificity for differentiating healthy controls from breast cancer patients. The same peak also demonstrated 70% sensitivity and 70% specificity in distinguishing patients with benign breast conditions from healthy individuals using saliva samples.

Additionally, the phosphate peak was notably higher in malignant tissues compared to fibrocystic and benign forms, aligning with prior findings that link phosphate levels to nucleic acid activity in malignant transformations.[38,39] While phosphate demonstrated some diagnostic potential, it was less effective for overall tumor discrimination according to its AUC, sensitivity, and specificity metrics. Nonetheless, it showed promise in differentiating between fibrocystic and fibroadenoma tissues with sensitivity and specificity rates of 82% and 100%, respectively, though this contrasts with other studies reporting less than 90% for both metrics.[4,6] The carcinogenesis marker appeared to aid primarily in differentiating fibrocystic tissues from fibroadenoma,[23,24] which could prove revolutionary for benign variant characterization and diagnosis.

While this study demonstrates encouraging clinical potential, several limitations warrant cautious interpretation of the findings and restrict their broad applicability. These include a modest sample size and the potential for confounding biases, particularly stemming from uncontrolled pre-analytical and analytical variables during tissue block preparation. Future investigations should address these limitations by employing larger, prospectively controlled cohorts to validate these results.

Conclusions

The study examines the efficacy of ATR-FTIR spectroscopy in distinguishing between normal and abnormal breast tissues using specific peak ratios as biomarkers. The research highlights that certain biomarkers, particularly the nucleocytoplasmic marker, demonstrate remarkable diagnostic accuracy, achieving an AUC ranging from 0.9 to 1.0, with a sensitivity of 100% in differentiating normal, benign, and cancerous tissues. Glycogen is identified as the most effective discriminator between fibrocystic changes and fibroadenomas, also showing perfect sensitivity and specificity. However, there is a need for future research with larger sample sizes to validate these findings.

Acknowledgments

The authors are indeed grateful to Dr. Blessings Effiong (Biochemistry Department, University of Uyo, Akwa Ibom, Nigeria) for advice on analyzing a tissue section with ATR-FTIR, Dr. Waheed Oluogun, and Mr. Richard Oduru (LAUTECH Teaching Hospital, Osogbo) for technical support and assistance during sample collection.

Funding

None.

Conflict of interest

The authors have no conflict of interest related to this publication

Author contributions

Study concept and design (STA, CI), acquisition of data (STA, SI), analysis and interpretation of data (STA, CI, SI), drafting of the manuscript (STA), critical revision of the manuscript for important intellectual content (STA, CI, SI), administrative, technical, or material support (CI, SI), and study supervision (STA, CI). All authors have made significant contributions to this study and have approved the final manuscript.

Ethical statement

Ethical approval for the study was granted by the Research Ethics Committee of Ladoke Akintola University of Technology (LAUTECH), Osun, Nigeria, with reference number: UTH/REC/2022/09/649. The study was carried out with a waiver of informed consent for the use of archived, anonymized samples in accordance with the principles of the Declaration of Helsinki (as revised in 2024). The ethics committee agreed that this study did not require informed consent due to its retrospective nature and the minimal risk involved.

Data sharing statement

The spectra plots and receiver's operating characteristics (ROC) graphical formats (attached as supplementary materials) used in support of the findings of this study are included within the article.

References

[1] Kumar A, Abbas AK, Aster JC. Robbins Basic Pathology. Tenth Edition. Pennsylvania: Elsevier Philadelphia; 2018:736–747.
[2] Iyiola S, Enweani IB, Ngokere AAAA, Avwioro OG, Komolafe AO, Ekundina VO. Assessment of the Proliferation of Breast Cancer Cells among Women in Osogbo, Osun State, Nigeria. J Morphol Anat 2019;3(1):118.
[3] Obinaju BE, Martin FL. ATR-FTIR spectroscopy reveals polycyclic aromatic hydrocarbon contamination despite relatively pristine site characteristics: Results of a field study in the Niger Delta. Environ Int 2016;89-90:93–101. doi:10.1016/j.envint.2016.01.012, PMID: 26826366.
[4] Elshemey WM, Ismail AM, Elbialy NS. Molecular-Level Characterization of normal, benign, and malignant breast tissues using FTIR spectroscopy. J Med Biol Eng 2016;36(3):369–378. doi:10.1007/s40846-016-0133-0.
[5] Luo Y, Liu H, Wu C, Paraskevaidi M, Deng Y, Shi W, *et al*. Diagnostic segregation of human breast tumours using Fourier-transform infrared spectroscopy coupled with multivariate analysis: Classifying cancer subtypes. Spectrochim Acta A Mol Biomol Spectrosc 2021;255:119694. doi:10.1016/j.saa.2021.119694, PMID:33799187.
[6] Ferreira ICC, Aguiar EMG, Silva ATF, Santos LLD, Cardoso-Sousa L, Araújo TG, *et al*. Attenuated Total Reflection-Fourier Transform Infrared (ATR-FTIR) Spectroscopy Analysis of Saliva for Breast Cancer Diagnosis. J Oncol 2020;2020:4343590. doi:10.1155/2020/4343590, PMID:32104176.
[7] Alhajjeh R, Al-Ali H. Application of FTIR spectroscopy method for the quantification of ascorbic acid in bulk materials and pharmaceutical formulation.Iraqi J Pharm Sci. 2023;32(3):186–194. doi:10.31351/vol32iss3pp186-194.
[8] Farooq S, Zezell DM. Diabetes Monitoring through Urine Analysis Using ATR-FTIR Spectroscopy and Machine Learning. Chemosensors 2023;11(11):565. doi:10.3390/chemosensors11110565.
[9] Pang N, Yang W, Yang G, Yang C, Tong K, Yu R, *et al*. The utilization of blood serum ATR-FTIR spectroscopy for the identification of gastric cancer. Discov Oncol 2024;15(1):350. doi:10.1007/s12672-024-01231-6, PMID:39143357.
[10] Paraskevaidi M, Karim S, Santos M, Lima K, Crean S. The use of ATR-FTIR spectroscopy for the diagnosis of Alzheimer's disease using oral buccal cells. Appl Spectrosc Rev 2024;59(8):1021–1035. doi:10.1080/05704928.2023.2284283.
[11] Kęsik JJ, Paja W, Jakubczyk P, Khalavka M, Terlecki P, Iłżecki M, *et al*. Determination of spectroscopy marker of atherosclerotic carotid stenosis using FTIR-ATR combined with machine learning and chemometrics analyses. Nanomedicine 2024;62:102788. doi:10.1016/j.nano.2024.102788, PMID:39341479.
[12] Sitnikova VE, Kotkova MA, Nosenko TN, Kotkova TN, Martynova DM, Uspenskaya MV. Breast cancer detection by ATR-FTIR spectroscopy of blood serum and multivariate data-analysis. Talanta 2020;214:120857. doi:10.1016/j.talanta.2020.120857, PMID:32278436.
[13] Shehu UF, Awwalu S, Adeshina GO. FTIR analysis and antimicrobial evaluation of aqueous ethanol leaf extract and fractions of pavonia snegalensis (Cav.) listener (Malvaceae). J Curr Biomed Rep 2021;1(3)
[14] Amponsah IK, Boakye A, Orman E, Armah FA, Borquaye LS, Adjei S, *et al*. Assessment of some quality parameters and chemometric-assisted FTIR spectral analysis of commercial powdered ginger products on the Ghanaian market. Heliyon 2022;8(3):e09150. doi:10.1016/j.heliyon.2022.e09150, PMID:35846447.
[15] Njokunwogbu AN, Amarachukwu O, Ene FC, Iyioku MU, Enyi CN. Separation And Infrared (Ft-Ir) Characterization Of Aromatic Hydrocarbons From High Boiling Fractions (200 Oc) Of Nigeria Crude Oil (Using Trichloroethylene As The Eluant). Int J Res Appl Sci Eng Technol 2022;8(8):1–9.

[16] Ityo SD, Anhwange BA, Okoye PAC, Feka PD. Sensory, GC-MS and FTIR analysis of aqueous extract of hibiscus sabdarriffa and Vernonia amygdalina herbal tea with blends of ginger and lemon zest. J Chem Soc Nigeria 2023;48(4):662–676. doi:10.46602/jcsn.v48i4.907.
[17] Lazaro-Pachecho D, Shaaban A, Baldwin G, Titiloye NA, Rehman S, Rehman IU. Deciphering the structural and chemical composition of breast cancer using FTIR spectroscopy. Appl Spectrosc Rev 2020;57(3):234–248. doi:10.1080/05704928.2020.1843471.
[18] Lazaro-Pacheco D, Shaaban AM, Titiloye NA, Rehman S, Rehman IU. Elucidating the chemical and structural composition of breast cancer using Raman micro-spectroscopy. EXCLI J 2021;20:1118–1132. doi:10.17179/excli2021-3962, PMID:34345231.
[19] Olaiya DO, Alatise OI, Oketayo OO, Abiye OE, Obianjunwa EI, Balogun FA. Trace Element Analysis of Cancerous and Non-cancerous Breast Tissues of African Women in Southwest Nigeria Using Particle-Induced X-ray Emission Technique. Breast Cancer (Auckl) 2019;13:1178223419840694. doi:10.1177/1178223419840694, PMID:31037030.
[20] Cui L, Butler HJ, Martin-Hirsch PL, Martin FL. Aluminium foil as a potential substrate for ATR-FTIR, transflection FTIR, or Raman spectrochemical analysis of biological specimen. Anal methods 2016;8:481–487. doi:10.1039/C5AY02638E.
[21] Carson FL, Cappellano CH. Histotechnology: A Self Instructional Text. 4th ed. Chicago, Illinois: American Society College of Pathology press; 2019:264–282.
[22] Baker MJ, Trevisan J, Bassan P, Bhargava R, Butler HJ, Dorling KM, *et al*. Using Fourier transform IR spectroscopy to analyze biological materials. Nat Protoc 2014;9(8):1771–1791. doi:10.1038/nprot.2014.110, PMID:24992094.
[23] Sahu RK, Argov S, Salman A, Huleihel M, Grossman N, Hammody Z, *et al*. Characteristic absorbance of nucleic acids in the Mid-IR region as possible common biomarkers for diagnosis of malignancy. Technol Cancer Res Treat 2004;3(6):629–638. doi:10.1177/153303460400300613, PMID:15560721.
[24] Yu G, Xu JL, Niu Y, Zhang CZ, Zhang CP. Studies on breast tumor tissues with ATR-FTIR spectroscopy. In: Chance B, Chen MZ, Chiou AET, Luo QM (eds). Optics in Health Care and Biomedical Optics: Diagnostics and Treatment II, Vol. 5630. SPIE; 2005:796–801. doi:10.1117/12.576398.
[25] Kumar S, Verma T, Mukherjee R, Ariese F, Somasundaram K, Umapathy S. Raman and infra-red microspectroscopy: towards quantitative evaluation for clinical research by ratiometric analysis. Chem Soc Rev 2016;45(7):1879–1900. doi:10.1039/c5cs00540j, PMID:26497386.
[26] Yano K, Sakamoto Y, Hirosawa N, Tanooka S, Katayama H, Kumaido K, *et al*. Applications of fourier transform infrared spectroscopy, fourier transform infrared microscopy and near infrared spectroscopy to cancer research. J Spectrosc 2003;17(2-3):315–321. doi:10.1155/2003/329478.
[27] Bradley AP. The use of the area under the ROC curve in the evaluation of machine learning algorithms. Pattern Recognit 1997;30(7):1145–1159. doi:10.1016/S0031-3203(96)00142-2.
[28] Vrbin CM. Recommendations for reporting measures of diagnostic accuracy. Cytopathology 2023;34(3):185–190. doi:10.1111/cyt.13208, PMID:36648307.
[29] Shreffler J, Huecker MR, Shreffler J, Huecker MR. Diagnostic Testing Accuracy: Sensitivity, Specificity, Predictive Values and Likelihood Ratios. Treasure Island (FL): StatPearls Publishing; 2025. PMID:32491423.
[30] Çorbacıoğlu ŞK, Aksel G. Receiver operating characteristic curve analysis in diagnostic accuracy studies: A guide to interpreting the area under the curve value. Turk J Emerg Med 2023;23(4):195–198. doi:10.4103/tjem.tjem_182_23, PMID:38024184.
[31] Moore MJ, Sebastian JA, Kolios MC. Determination of cell nucleus-to-cytoplasmic ratio using imaging flow cytometry and a combined ultrasound and photoacoustic technique: a comparison study. J Biomed Opt 2019;24(10):1–10. doi:10.1117/1.JBO.24.10.106502, PMID:31625322.
[32] Sebastian JA, Moore MJ, Berndl ESL, Kolios MC. An image-based flow cytometric approach to the assessment of the nucleus-to-cytoplasm ratio. PLoS One 2021;16(6):e0253439. doi:10.1371/journal.pone.0253439, PMID:34166419.
[33] Andrus PG. Cancer monitoring by FTIR spectroscopy. Technol Cancer Res Treat 2006;5(2):157–167. PMID:16551135.
[34] Carton J. Oxford handbook of pathology. 3rd ed. Oxford: Oxford University Press; 2024:349–364.
[35] Zelig U, Barlev E, Bar O, Gross I, Flomen F, Mordechai S, *et al*. Early detection of breast cancer using total biochemical analysis of peripheral blood components: a preliminary study. BMC Cancer 2015;15:408. doi:10.1186/s12885-015-1414-7, PMID:25975566.
[36] Wang H, Logan DT, Danielsson J, Oliveberg M. Exposing the distinctive modular behavior of β-strands and α-helices in folded proteins. Proc Natl Acad Sci U S A 2020;117(46):28775–28783. doi:10.1073/pnas.1920455117, PMID:33148805.
[37] Dannhorn A, Swales JG, Hamm G, Strittmatter N, Kudo H, Maglennon G, *et al*. Evaluation of Formalin-Fixed and FFPE Tissues for Spatially Resolved Metabolomics and Drug Distribution Studies. Pharmaceuticals (Basel) 2022;15(11):1307. doi:10.3390/ph15111307, PMID:36355479.
[38] Amjad M, Ullah H, Andleeb F, Batool Z, Nazir A, Gilanie G. Fourier transform infrared spectroscopy for investigation of human carcinoma and leukaemia. Lasers Eng 2021;51(1-5):217–233.
[39] Depciuch J, Barnaś E, Skręt-Magierło J, Skręt A, Kaznowska E, Łach K, *et al*. Spectroscopic evaluation of carcinogenesis in endometrial cancer. Sci Rep 2021;11(1):9079. doi:10.1038/s41598-021-88640-7, PMID:33907297.
[40] Ghimire H, Garlapati C, Janssen EAM, Krishnamurti U, Qin G, Aneja R, *et al*. Protein Conformational Changes in Breast Cancer Sera Using Infrared Spectroscopic Analysis. Cancers (Basel) 2020;12(7):1708. doi:10.3390/cancers12071708, PMID:32605072.
[41] Yousif ES, Fawaz NI, Mohamed BJ. Human breast tissue cancer diagnosis by FT-IR spectroscopy. Journal of University of Anbar for Pure Science 2015;9(3):19–26. doi:10.37652/juaps.2015.127546.